Fibroblast Growth Factor 21 Protects Photoreceptor Function in Type 1 Diabetic Mice

Zhongjie Fu,[1] Zhongxiao Wang,[1] Chi-Hsiu Liu,[1] Yan Gong,[1] Bertan Cakir,[1] Raffael Liegl,[1] Ye Sun,[1] Steven S. Meng,[1] Samuel B. Burnim,[1] Ivana Arellano,[1] Elizabeth Moran,[1] Rubi Duran,[1] Alexander Poblete,[1] Steve S. Cho,[1] Saswata Talukdar,[2] James D. Akula,[1] Ann Hellström,[3] and Lois E.H. Smith[1]

Diabetes 2018;67:974–985 | https://doi.org/10.2337/db17-0830

COMPLICATIONS

Retinal neuronal abnormalities occur before vascular changes in diabetic retinopathy. Accumulating experimental evidence suggests that neurons control vascular pathology in diabetic and other neovascular retinal diseases. Therefore, normalizing neuronal activity in diabetes may prevent vascular pathology. We investigated whether fibroblast growth factor 21 (FGF21) prevented retinal neuronal dysfunction in insulin-deficient diabetic mice. We found that in diabetic neural retina, photoreceptor rather than inner retinal function was most affected and administration of the long-acting FGF21 analog PF-05231023 restored the retinal neuronal functional deficits detected by electroretinography. PF-05231023 administration protected against diabetes-induced disorganization of photoreceptor segments seen in retinal cross section with immunohistochemistry and attenuated the reduction in the thickness of photoreceptor segments measured by optical coherence tomography. PF-05231023, independent of its downstream metabolic modulator adiponectin, reduced inflammatory marker interleukin-1β (IL-1β) mRNA levels. PF-05231023 activated the AKT-nuclear factor erythroid 2–related factor 2 pathway and reduced IL-1β expression in stressed photoreceptors. PF-05231023 administration did not change retinal expression of vascular endothelial growth factor A, suggesting a novel therapeutic approach for the prevention of early diabetic retinopathy by protecting photoreceptor function in diabetes.

Diabetic retinopathy (DR) is a common complication of diabetes. The incidence of DR worldwide is projected to increase to >190 million by 2030, and the number of individuals with vision-threatening proliferative DR will likely increase to >56 million (1). In DR, retinal neovascularization occurs late (proliferative DR), induced by earlier vessel loss (nonproliferative DR). Current treatments targeting retinal neovascularization have limitations. Clinical trials of anti–vascular endothelial growth factor (VEGF) drugs for DR suggests efficacy in some but not all patients. There are also safety concerns about the long-term anti-VEGF drug effects, including degeneration of normal blood vessels and choroid as well as degeneration of neural retina (2). New therapeutic approaches to prevent early retinal vessel loss to avoid the blinding end stage of DR would be of great benefit. Retinal neural electrophysiological dysfunction occurs early before vascular abnormalities in DR (3). Therefore, maintaining normal retinal function may help to prevent DR progression.

Increased oxidative stress from hyperglycemia-associated metabolic abnormalities is involved in the development of diabetic retinal microvascular changes (4). The retina is a highly metabolically demanding tissue, and photoreceptors have the highest number of mitochondria of any cell in the body (5). Of all retinal cells, photoreceptors contribute the most to diabetes-induced retinal oxidative stress and inflammation in mice (6). Superoxide production is increased in diabetic photoreceptors (7). It has been shown that photoreceptors can control retinal vascular development. In patients with diabetes who have proliferative retinopathy and later development of retinitis pigmentosa (a photoreceptor-degenerative disease), retinal neovascularization (DR) slowly regresses (8). Therefore, enhancing the antioxidant pathways in photoreceptors may prevent neurovascular damage in DR.

[1]Department of Ophthalmology, Boston Children's Hospital, Harvard Medical School, Boston, MA
[2]Merck Research Laboratories, Boston, MA
[3]Section for Ophthalmology, Department of Clinical Neuroscience, Institute of Neuroscience and Physiology, Sahlgrenska Academy, University of Gothenburg, Göteborg, Sweden

Corresponding author: Lois E.H. Smith, lois.smith@childrens.harvard.edu.

Received 14 July 2017 and accepted 7 February 2018.

This article contains Supplementary Data online at http://diabetes.diabetesjournals.org/lookup/suppl/doi:10.2337/db17-0830/-/DC1.

Fibroblast growth factor 21 (FGF21) improves metabolic homeostasis in diabetes (9). FGF21 is expressed in many tissues, although circulating FGF21 under physiological conditions is derived mainly from the liver (10). FGF21 levels in patients with type 1 diabetes are lower than in healthy control subjects (11,12). FGF21 has not been extensively studied in DR, although there is evidence in other systems to suggest that it could be important. In type 1 diabetic mice, FGF21 protects against diabetes-induced testicular apoptotic cell death and renal dysfunction (13,14) and prevents diabetic nephropathy (15) through activation of the nuclear factor erythroid 2–related factor 2 (NRF2) pathway. NRF2 upregulates antioxidant enzyme expression and is a critical defense mechanism against oxidative stress in the retina (16). We previously found that FGF21 decreases pathological retinal vessel proliferation and promotes physiological retinal vascularization in mouse oxygen-induced retinopathy (OIR), modeling late proliferative DR (17). However, there is limited knowledge of the role of FGF21 in early DR. We investigated whether FGF21 protection against early retinal neuronal dysfunction in diabetes in the following two mouse models of type 1 diabetes: *1*) insulin-deficient Akita mice; and *2*) streptozotocin (STZ)-induced diabetic mice. We found that the administration of a long-acting FGF21 analog, PF-05231023, improved photoreceptor dysfunction and morphology, as well as reduced retinal inflammation in vivo and in vitro.

RESEARCH DESIGN AND METHODS

Study Approval

All animal studies adhered to the Association for Research in Vision and Ophthalmology Statement for the Use of Animals in Ophthalmic and Vision Research and were approved by the Institutional Animal Care and Use Committee at Boston Children's Hospital.

Mouse Models of Type 1 Diabetes

Akita Mice

Ins2^{Akita} male mice have a spontaneous mutation in the insulin 2 gene, which leads to incorrect folding of insulin protein. Heterozygous Akita mice develop diabetes within 1 month and retinal complications at ~6 months of age (18). The 7- to 8-month-old Akita mice were compared with littermate wild-type (WT) mice. Akita mice with retinal functional abnormalities were screened with electroretinography (ERG) and those with ERG changes were intraperitoneally injected with 10 mg/kg long-acting FGF21 analog PF-05231023 (Pfizer) or vehicle control twice a week for 4 weeks. Retinal function was again examined with ERG after 4 weeks of treatment, and body weight and blood glucose were recorded. Serum triglyceride levels were measured using the Wako L-Type TG M test.

STZ-Induced Diabetic Mice

The 6- to 8-week-old male WT and adiponectin (APN)-deficient (*Apn*$^{-/-}$) mice were starved 6 h prior to an intraperitoneal injection of 55 mg/kg/day STZ on days 1 and 2 followed by an injection of 60 mg/kg/day STZ from day 3 to 5. Diabetes was induced within 1 week of injection (18). The 7- to 8-month-old diabetic WT and *Apn*$^{-/-}$ mice were screened with ERG. Mice with retinal functional abnormalities were intraperitoneally injected with 10 mg/kg PF-05231023 or vehicle control twice a week for 4 weeks. Retinal function was then re-examined with ERG.

ERG

ERG was used to assess the function of retinal neurons. Flash ERGs were obtained using an Espion e^2 (Diagnosys LLC, Lowell, MA) in dark-adapted, mydriatic (Cyclomydril; Alcon, Fort Worth, TX), anesthetized (ketamine/xylazine) subjects. Stimuli were "green" light-emitting diode flashes of doubling intensity from ~0.0064 to ~2.05 cd·s/m^2 and then "white" xenon-arc flashes from ~8.2 to ~1,050 cd·s/m^2 presented in an integrating sphere (Colordome; Diagnosys LLC). As shown (Fig. 2*A*), the saturating amplitude (Rm_{P3}) and sensitivity (*S*) of the rod photoreceptors was estimated from the *a*-waves elicited by the white flashes (19). The bipolar cell response amplitude and sensitivity ($1/K_{P2}$) of second-order neurons, principally bipolar cells (20), was measured by subtracting this model from the intact ERG waveform (21) and fitting the Naka-Rushton equation (22) to the response versus intensity relationship of the resulting waveform "P2." The oscillatory potentials (OPs), which characterize activity in inner retinal cells distinct from the generators of the *a*- and *b*-waves (23), were filtered from P2 (24) and assessed in the frequency domain to determine their energy (25); the saturating energy (*Em*) and sensitivity ($1/i_{1/2}$) of the OPs were then assessed in a similar manner as those of P2. Finally, retinal sensitivity at threshold (*Sm*) was calculated by scaling the amplitude of each P2 by the intensity used to elicit it and fitting a generalized logistic growth curve, with the exponent set to negative unity, to the resulting sensitivities and determining the limit of this function as intensity approached zero (26).

Optical Coherence Tomography

Mice were anesthetized (ketamine/xylazine), and their pupils were dilated (Cyclomydril; Alcon). Spectral domain optical coherence tomography (OCT) with the guidance of a bright-field live fundus image was performed with the image-guided OCT system (Micron IV; Phoenix Research Laboratories). Photoreceptor inner and outer segment thicknesses were measured using Insight (provided by Micron IV). The thickness of photoreceptor segments was plotted at six distances (50, 100, 150, 200, 250, and 300 μm) from the optic nerve head both on the nasal and on the temporal side.

Immunohistochemistry

For immunohistochemistry on retinal cross sections, eyes were fixed in 4% paraformaldehyde, frozen in optimal cutting temperature compound (Tissue-Tek), and then cut into 10-μm sections and rinsed with PBS. The sections with optic nerve were treated with ice-cold methanol for 15 min and then 0.1% triton PBS for 45 min at room temperature. The sections were blocked with 3% BSA for 1 h at room temperature and stained with primary antibody against cone

arrestin (1:500; catalog #AB15282; Millipore) and rhodopsin (1:500; MABN15; Millipore) overnight at 4°C. The sections were stained with corresponding secondary antibody, covered in mounting medium with DAPI (H-1200; Vector Laboratories), and visualized with a Leica SP2 Confocal Microscope or a Zeiss AxioObserver.Z1 Microscope at 200× magnification.

Laser-Captured Microdissection

Fresh mouse eyes were embedded in optimal cutting temperature compound and sectioned at 12 μm in a cryostat, mounted on RNase-free polyethylene naphthalate glass slides (catalog #11505189; Leica). Frozen sections were fixed in 70% ethanol for 15 s, followed by 30 s in 80% ethanol and 30 s in absolute ethanol, and then washed with diethyl pyrocarbonate–treated water for 15 s. Laser dissection of retinal neuronal layers was performed immediately thereafter with the Leica LMD 6000 System (Leica Microsystems), and samples were collected directly into lysis buffer from the RNeasy Micro Kit (Qiagen, Chatsworth, CA).

Photoreceptors (661 W) Cell Culture

Photoreceptor 661 W cells were cultured at 37°C, with 5% CO_2 in a humidified atmosphere in DMEM (catalog #1196502; Gibco) supplemented with 10% FBS (catalog #S12450; Atlanta Biologicals) and 1% antibiotic/antimycotic solution. An equal number of cells per well was plated on a six-well dish. Oxidative stress was induced with 0.5 mmol/L paraquat (PQ; catalog #856177; Sigma-Aldrich) for 1 h at 37°C. The culture media were changed, and the cells were treated with vehicle (PBS) or 500 ng/mL PF-05231023 for 24 h. Cells were collected for protein and RNA.

Real-time PCR

Retinas or 661 W cells were lysed with QIAzol lysis reagent and incubated on ice for 15 min. Chloroform 20% was added and incubated for 5 min at room temperature. RNA was extracted according to the manufacturer instructions using a PureLink RNA Mini Kit (catalog #12183018A; Ambion). RNA was then reverse transcribed using iScript cDNA Synthesis Kit (catalog #1708891; Bio-Rad). Quantitative PCR (qPCR) was performed for the following: *Arrestin4*: 5′-GAG CAA GGG CTG CTA CTC AAG-3′, 5′-AAC CGC AGG TTC AAG TAT TCC-3′; *Rhodopsin*: 5′-TCA TGG TCT TCG GAG GAT TCA C-3′, 5′-TCA CCT CCA AGT GTG GCA AAG-3′; *IL-1β*: 5′-TTC AGG CAG GCA GTA TCA CTC-3′, 5′-GAA GGT CCA CGG GAA AGA CAC-3′; *IL-6*: 5′-TAG TCC TTC CTA CCC CAA TTT CC-3′, 5′-TTG GTC CTT AGC CAC TCC TTC-3′; *Vegfa* F: 5′-GGA GAT CCT TCG AGG AGC ACT T-3′, R: 5′-GCG ATT TAG CAG CAG ATA TAA GAA-3′; *Tnfα* 5′-CAT CTT CTC AAA ATT CGA GTG ACA A-3′, 5′-TGG GAG TAG ACA AGG TAC AAC CC-3′; *IL-10*: 5′-CTT ACT GAC TGG CAT GAG GAT CA-3′, 5′-GCA GCT CTA GG AGC ATG TGG-3′; *Apn:* 5′-GAA GCC GCT TAT GTG TAT CGC-3′, 5′-GAA TGG GTA CAT TGG GAA CAG T-3′; *Nrf2*: 5′-TAG ATG ACC ATG AGT CGC TTGC-3′, 5′-GCC AAA CTT GCT CCA TGT CC-3′; and *Nfκb*: forward, 5′-GGA GAG TCT GAC TCT CCC TGA GAA-3′, reverse, 5′-CGA TGG GTT CCG TCT TGG T-3′. Quantitative analysis of gene expression was generated using an Applied Biosystems 7300 Sequence Detection System with the SYBR Green Master Mix Kit, and gene expression was calculated relative to *cyclophilin A* (5′-CAG ACG CCA CTG TCG CTT T-3′; 5′-TGT CTT TGG AAC TTT GTC TGC AA-3′) (retinas) or *β-actin* (5′-CGG TTC CGA TGC CCT GAG GCT CTT-3′, 5′-CGT CAC ACT TCA TGA TGG AAT TGA-3′) (photoreceptor 661 W cells) using the ΔΔCt method. Each sample was repeated in triplicate.

Western Blot

Five microliters of protein lysate from photoreceptor 661 W cells were used to detect the levels of NRF2 (1:500; MAB3925; R&D Systems), phospho (p)–nuclear factor-κB (NF-κB) (1:200; catalog #3037S; Cell Signaling Technology), NF-κB (1:1,000; catalog #3034; Cell Signaling Technology), p-AKT (1:500; catalog #9271; Cell Signaling Technology), AKT (1:1,000; catalog #4691; Cell Signaling Technology) in 5% BSA overnight at 4°C. Signals were detected using 1:5,000 corresponding horseradish peroxidase–conjugated secondary antibodies and enhanced chemiluminescence (Pierce), then the digital images were visualized with a Bio-Rad ChemiDoc Touch Imaging System. β-Actin (1:5,000; catalog #A1978; Sigma-Aldrich) was used as internal control.

Statistical Analysis

All ERG data were presented as the log change from control (ΔLogNormal); by expressing the data in log values, changes in observations of fixed proportion become linear, consistent with a constant fraction for physiologically meaningful changes in parameter values (26). ΔLogNormal ERG data were plotted as the mean ± SEM and evaluated for significant effects using mixed-effects linear models (MLMs) (27). In each analysis, two MLMs were used. The first MLM, carried out on the saturating *a*-wave, P2, and OP parameters, had group (Akita vs. WT; or STZ vs. control), treatment (before vs. after PF-05231023 administration), parameter (amplitude vs. sensitivity), and retinal depth (photoreceptor vs. bipolar vs. inner retina). The second MLM, carried out on *Sm*, had factors group and treatment. Data from both eyes were included in all analyses. Differences in ERG parameters were detected by ANOVA followed by Tukey test. Two-tailed unpaired *t* test and ANOVA with Bonferroni multiple-comparison test were used for comparison of results as specified (Prism version 5.0; GraphPad Software, Inc., San Diego, CA). The threshold for statistical significance (α) was set at 0.05.

RESULTS

PF-05231023 Administration Restored Retinal Function in Akita Mice

Circulating FGF21 levels (ELISA) were reduced in >7-month-old Akita mice compared with littermate WT control mice (Fig. 1*A*). Retinal expression of *Fgf21* (qPCR) was not changed significantly (Fig. 1*B*). The physiological and pharmacological actions of FGF21 are dependent on the receptor FGFR1 and the coreceptor β-klotho (28,29). The gene expression of FGF21 receptor *Fgfr1* was comparable in Akita versus WT mouse retinas and that of *β-klotho* was mildly increased

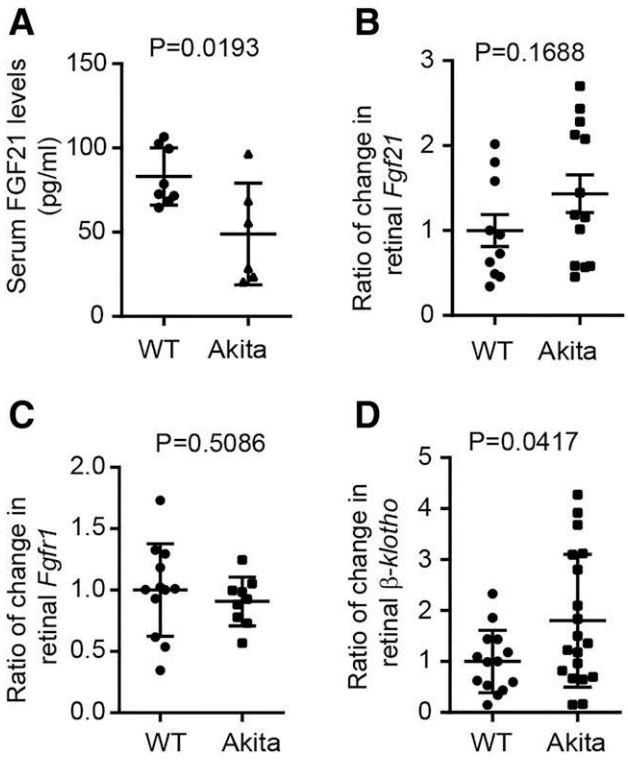

Figure 1—Serum FGF21 levels were decreased in Akita mice. *A*: ELISA measurement of serum FGF21. n = 6–8 mice/group. *B–D*: qPCR for *Fgf21, Fgfr1, β-klotho* expression in diabetic WT and Akita retinas. n = 9–19 replicates from three to four mice per group. The expression of genes was first compared with internal control *cyclophilin A*. Ratio indicates the ratio of gene to *cyclophilin A* normalized to WT ratio. Unpaired t test was used, and data are presented as the mean ± SD.

(Fig. 1*C* and *D*) (28,29). *Fgfr1* was expressed in retinal neurons isolated from retinal cross sections with laser-captured microdissection (Supplementary Fig. 1).

To examine whether FGF21 protects against retinal dysfunction in DR, we first administered PF-05231023 (10 mg/kg intraperitoneally, twice a week for a month) or vehicle control to those Akita mice that had ERG deficits at 7–8 months of age (50% of Akita mice [6 of 12 mice] had ERG deficits compared with their age-matched WT control mice). In Akita mice with ERG deficits, PF-05231023 administration did not change the body weight and serum triglyceride levels versus controls but mildly reduced blood glucose levels (Supplementary Fig. 2). Prior to PF-05231023 treatment, we examined ERG responses in Akita mice. Although the Akita mouse responses were slightly attenuated overall compared with WT controls (Fig. 2*A–C*), *Sm*, as determined by mixed-linear modeling, was significantly attenuated (F = 15.9; df = 1,27.0; P = 0.00046) relative to WT. PF-05231023 showed protective effects on Akita retinas (Fig. 2*B* and *C*). Notably, *Sm* in Akita mice was improved after treatment (Fig. 2*D*) (F = 27.9, df = *1,29.8*, $P = 1.1 \times 10^{-5}$) to levels that were supranormal, a result of better *a*-wave (log S) and *b*-wave (log $1/K_{P2}$) sensitivities (Fig. 2*E*). There was no decline in baseline retinal function (ERG signals) in any individual mouse between 7 and 8 months of age (F = 0.166, df = 1,2, P = 0.723) (Supplementary Fig. 3). In Akita mice, the change in postreceptor sensitivity (log $1/K_{P2}$) was positively correlated with the sum of changes in photoreceptor sensitivity and saturated amplitudes (log S + log Rm_{P3}, *a*-wave) (Fig. 3*A*), suggesting that the changes in postreceptor cells were reflecting the deficits in photoreceptor function (30,31).

PF-05231023 Administration Restored Photoreceptor Morphology in Akita Mice

In addition to neuronal function, we examined whether cone and rod photoreceptor structure was influenced by PF-05231023 administration. PF-05231023 administration increased cone-specific *arrestin4* expression (32) and did not change rhodopsin expression at the mRNA levels in Akita mice (Fig. 3*B*). Color vision is initiated by a G-protein–coupled receptor–mediated phototransduction cascade in cones. Arrestins bind to the phosphorylated G-protein–coupled receptors and rapidly desensitize the activated receptors (32), contributing to the maintenance of photoreceptor function and health. Cone-specific arrestin 4 deficiency leads to diminished visual acuity and contrast sensitivity, as well as to significantly reduced neuronal responses detected by ERG in mice (33). Cone photoreceptor outer and inner segments were oriented in parallel in WT mice but were disorganized in Akita mice. PF-05231023 administration normalized the photoreceptor segment arrangement (Fig. 3*C*). Rhodopsin staining was comparable between WT and PF-05231023-treated Akita mouse retinas, whereas there appeared to be a reduction in the thickness of rod photoreceptor segments in Akita mice (Fig. 3*D*). With OCT measurements, there was a significant reduction in the total thickness of photoreceptor inner and outer segment in Akita mice (blue line) versus WT mice (black line), but the reduction in the inner and outer segment thickness was no longer observed with PF-05231023 administration (orange line) (Fig. 3*E*). These observations suggest that PF-05231023 protection against DR takes place through the restoration of photoreceptor function and structure. We do not exclude the possibility of the contribution from other retinal cells as *Fgfr1* is also expressed in the inner nuclear layer and retinal ganglion cell (Supplementary Fig. 1).

PF-05231023 Decreased Retinal Inflammation in Diabetic Mice

Retinal inflammation induces retinal neurovascular abnormalities in diabetes (6,7,34,35). Significantly increased retinal *IL-1β* and decreased *Vegfa* mRNA expression was observed in Akita versus WT mice (Fig. 4*A*). PF-05231023 administration reduced retinal *IL-1β* mRNA expression in Akita mice (Fig. 4*B*). Interleukin (IL)-1β inhibits energy production in retinal neurons and induces retinal microvascular changes in rats (36–38). PF-05231023 administration did not change the expression levels of *Vegfa*, *Tnfα*, *IL-6*, *IL-10*, and *Apn* in Akita mouse retinas (Fig. 4*B*).

PF-05231023 Inhibited Oxidative Stress–Induced Inflammation in Photoreceptors

Hyperglycemia induces oxidative stress, a crucial contributor to DR (39). Photoreceptors are the most metabolically

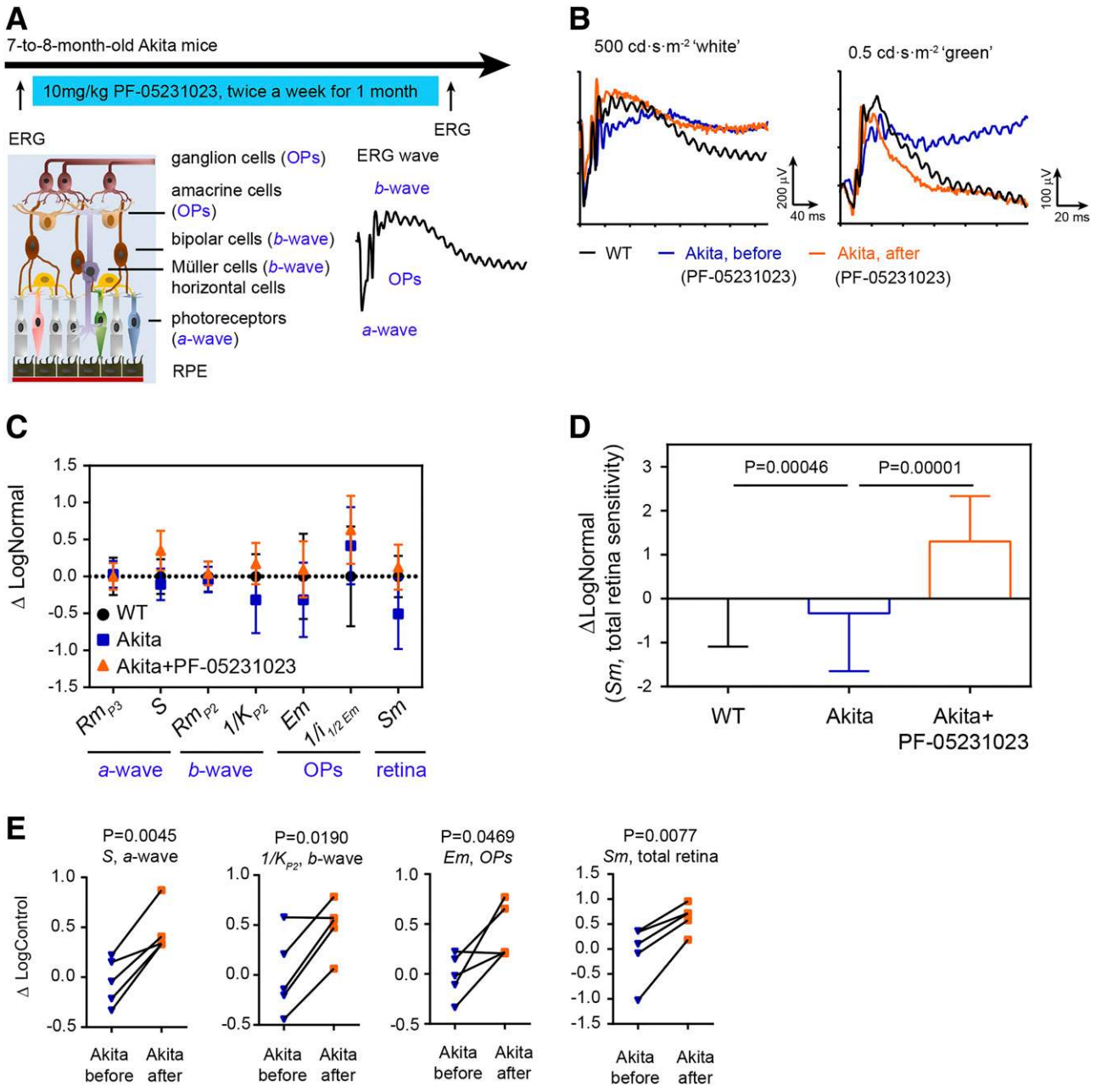

Figure 2—PF-05231023 administration improved retinal function in diabetic Akita mice. *A*: Schematic of PF-05231023 treatment in 7- to 8-month-old Akita mice. A dose of 10 mg/kg PF-05231023 was intraperitoneally injected twice a week for a month. ERG was measured before and after treatment. ERG plots with "white" (for maximal *a*-wave) and "green" (for maximal *b*-wave) light stimulation are shown to demonstrate the parameters: *a*-wave (photoreceptors), *b*-wave (bipolar cells), and OPs (inner retinal neurons). Rm_{P3}, *S*, bipolar cell response amplitude (Rm_{P2}), $1/K_{P2}$, inner retinal neuronal *Em*, $1/i_{1/2Em}$, as well as total *Sm* were measured and calculated. *B*: Representative ERG plots in 7- to 8-month-old WT mice (black) and age-matched Akita mice before (blue) and after (orange) PF-05231023 administration. *C*: Overall changes in different ERG parameters in WT mice, and in Akita mice before and after PF-05231023 administration. $n = 10–18$ eyes from 5–10 mice/group. *D*: Comparison of *Sm* in WT mice, and Akita mice before and after PF-05231023 administration. $n = 10–18$ eyes from 5–10 mice/group. ANOVA followed by Tukey test. *E*: Plots of ERG parameters in 7- to 8-month-old Akita mice before and after PF-05231023 administration. $n = 5$ mice/group. Paired *t* test was used, and data are presented as the mean ± SEM.

active cell in the body, and are very susceptible to metabolic derangement and resulting oxidative stress (40). Modulating photoreceptor oxidative stress protects against retinal neurodegeneration (41). In PF-05231023–treated versus vehicle-treated Akita mouse retinas, there was a significant increase in total AKT levels, although there was no significant change in the ratio of p-AKT to AKT (Fig. 5*A*), suggesting that the absolute level of p-AKT was higher in PF-05231023–treated mouse retinas. Activation of the AKT pathway regulates NRF2 activity in retinal pigment epithelium in vitro (42). There was a large variation of NRF2 protein levels in Akita versus WT mice. PF-05231023 administration decreased

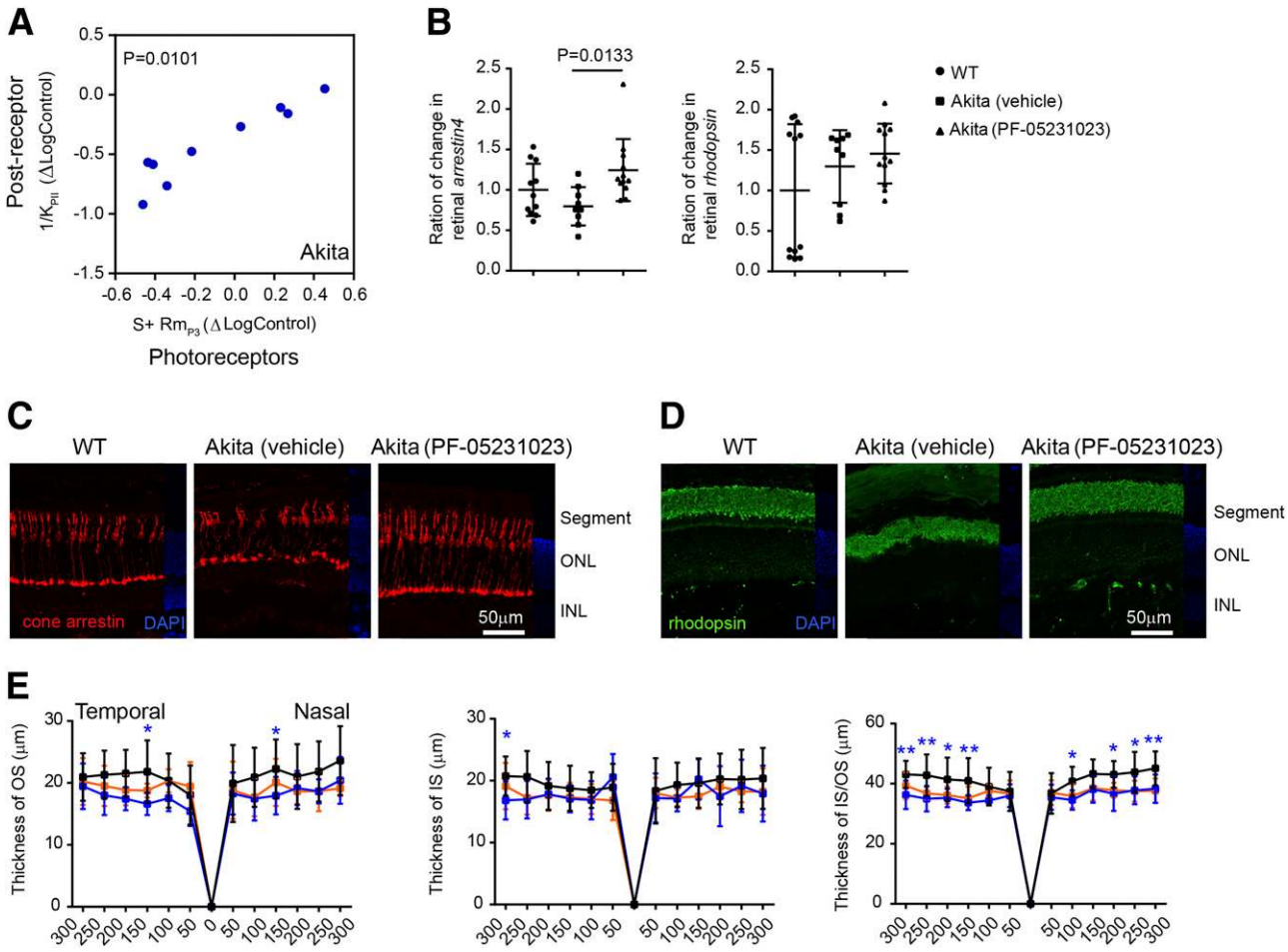

Figure 3—PF-05231023 administration restored the retinal morphology in Akita mice. *A*: Correlation of $1/K_{P2}$ with the sum of changes in S and Rm_{p3} in Akita mice. n = 10 eyes/group. Pearson r test. *B*: qPCR of *arrestin4* and *rhodopsin* in age-matched WT mice and Akita mice treated with either vehicle or PF-05231023. n = 9–12 replicates from three to four mice per group. The expression of genes was first compared with internal control *cyclophilin A*. Ratio indicates the ratio of gene to *cyclophilin A* normalized to WT ratio; ANOVA was used. *C* and *D*: Immunohistochemistry of cones (cone arrestin, red), rods (rhodopsin, green), and nuclei (DAPI, blue) in age-matched WT mice and Akita mice treated with either vehicle or PF-05231023. INL, inner nuclear layer; ONL, outer nuclear layer. Scale bar, 50 μm. *E*: OCT for photoreceptor inner and outer segment in age-matched WT mice (black line) and Akita mice treated with either vehicle (blue line) or PF-05231023 (orange line). IS, inner segment; OS, outer segment. n = 6–19 eyes from 4–10 mice/group. $^*P < 0.05$; $^{**}P < 0.01$ Akita heterozygous vs. WT mice. ANOVA was used; data are presented as the mean ± SD.

the variability of retinal NRF2 levels (Fig. 5*B*, blot 1) and showed a trend (nonsignificant) toward increased NRF2 levels (Fig. 5*B*, blot 2) in Akita mice. Taken together, the results suggested that PF-05231023 modulates retinal NRF2 levels by activating the AKT pathway. We further validated the observation in 661 W cells in vitro. We first evaluated the effect of hyperglycemia on 661 W cells. The 661 W cells tolerate very high levels of glucose (up to 100 mmol/L, in which 40% of total medium volume is glucose [stock is 555 mmol/L]) (Supplementary Fig. 4). The higher the glucose level, the more osmotic stress is induced. Hyperglycemia induces retinal oxidative stress, a crucial contributor leading to DR (39). Oxidative stress, resulting from highly metabolic photoreceptors, induces inflammation, which induces DR (6,7,34,35,40). Modulating oxidative stress prevents the progression of DR (43). The NRF2 pathway has antioxidant capability (41) and regulates *IL-1β* transcription (44,45). Therefore, we induced oxidative stress alone instead of inducing hyperglycemia with osmotic stress in 661 W cells for further confirmation of the mechanism. To test whether PF-05231023 protects photoreceptors against oxidative stress, we induced oxidative stress with the use of PQ, a nonselective herbicide, to induce the production of reactive oxygen species in mitochondria (46). In 661 W cells (the only photoreceptor cell line available currently) in vitro, oxidative stress induced with PQ increased *IL-1β* expression; PF-05231023 treatment prevented *IL-1β* induction (Fig. 5*C*). Both the activation of antioxidant transcriptional factor NRF2 and the phosphorylation of NF-κB modulate IL-1β transcription, which can be modulated by FGF21 (44,45,47). PF-05231023 treatment increased gene expression of *Nrf2* but not *Nfκb* in 661 W (Fig. 5*D*). In PQ-treated 661 W cells (to induce oxidative stress), the induction of NRF2 expression by PF-05231023 was dose-dependently inhibited by perifosine, an

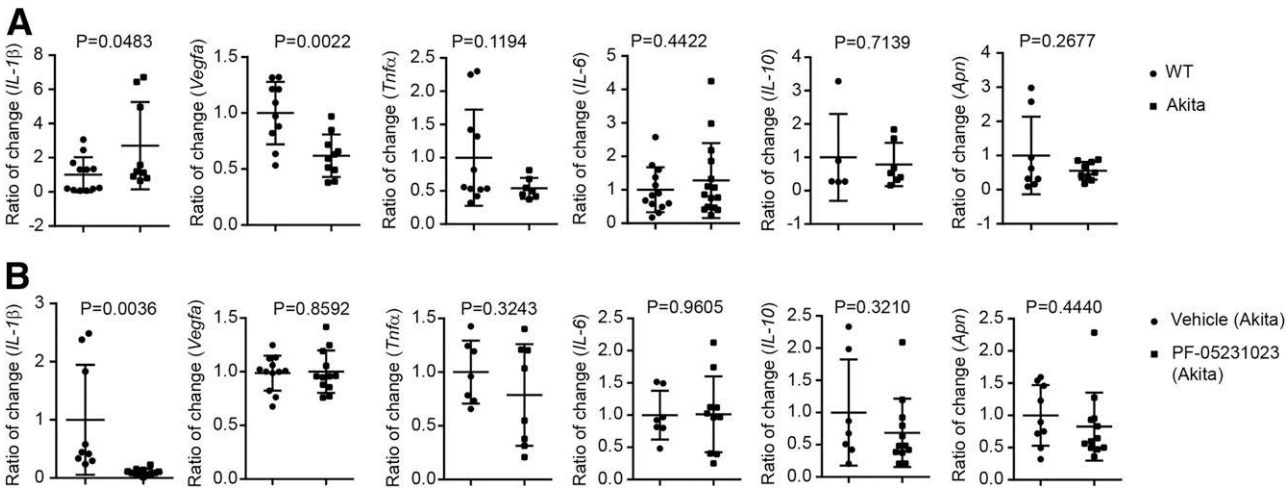

Figure 4—PF-05231023 administration decreased IL-1β expression in diabetic retinas. qPCR for proinflammatory markers (*IL-1β*, *Vegfa*, *Tnfα*, *IL-6*) and anti-inflammatory markers (*IL-10*, *Apn*). *A*: WT and Akita mouse retinas. n = 5–23 replicates from three to four mice per group. *B*: Akita mouse retinas treated with vehicle (PBS) or PF-05231023. n = 7–12 replicates from three to four mice per group. The expression of genes was first compared with internal control *cyclophilin A*. Ratio indicates the ratio of gene to *cyclophilin A* normalized to control ratio (WT in *A*, Akita with PBS in *B*). Data are presented as the mean ± SD; unpaired t test.

AKT inhibitor (48) (Fig. 5*E*). PQ induced NRF2 protein levels and PF-05231023 treatment further increased NRF2 production, but did not change NF-κB phosphorylation in photoreceptors with PQ-induced oxidative stress (Fig. 5*F*). Cell antioxidant systems control reactive oxygen species for cell survival (49). PQ induces an increase in cellular reactive oxygen species (46). As a response, cells may induce their antioxidant levels as a defense, such as inducing NRF2 expression (Fig. 5*F*). PF-05231023 further increased NRF2 protein levels, suggesting further protection against oxidative stress.

PF-05231023 Administration Protected STZ-Induced Diabetic Mice Against DR, Partly Independent of APN

APN is a key mediator of FGF21 modulation of glucose and lipid metabolism in mice (50,51). Changes in the APN pathway may contribute to the development of neovascular eye diseases (52). To test whether APN mediated the protective effects of PF-05231023, diabetes was induced with an injection of STZ in 6- to 8-week-old WT and $Apn^{-/-}$ mice. Retinal function was then examined by ERG at 7–8 months of age. Again, PF-05231023 administration did not change body weight, blood glucose levels, or serum triglyceride levels (Supplementary Fig. 5). Furthermore, neither the amplitude nor sensitivity of the *a*-wave, *b*-wave, or the OPs differed significantly between STZ-treated mice (Fig. 6*A–C*), but *Sm* was significantly attenuated after STZ treatment (F = 12.2, df = 1,6.0, P = 0.013) (Fig. 6*D*). PF-05231023, administered as described above, again improved log *Sm* values (F = 45.2, df = 1,5.9, P = 0.001) in the STZ-treated mice to levels that were supranormal (Fig. 6*D* and *E*). The protective effects of PF-05231023 on retinal sensitivity (log *Sm*) in STZ-induced WT diabetic mice were again found in $Apn^{-/-}$ diabetic mice (F = 23.8, df = 1,2, P = 0.040) (Fig. 6*F–H*), suggesting that the rescue was partly independent of APN. In the STZ-induced diabetic mice, PF-05231023 decreased *IL-1β* expression in diabetic WT and $Apn^{-/-}$ retinas (Fig. 6*I*), suggesting that PF-05231023–induced reduction in *IL-1β* was independent of APN, in line with our phenotypic observation cited above (Fig. 6*F–H*).

DISCUSSION

New therapeutic approaches to prevent and manage DR are needed. Dysfunction in photoreceptors and postreceptor neurons are among the early retinal changes seen in patients with diabetes, anteceding ophthalmoscopic signs of retinopathy (3). In diabetes, hyperglycemia causes oxidative stress, a crucial inducer of DR (39). Activation of the antioxidant protein NRF2 protects against retinal neuronal degeneration (41), particularly in photoreceptors, as photoreceptors are the most metabolically active cells in the body (53,54) and are more vulnerable to oxidative stress damage. Our study demonstrated that, in insulin-deficient diabetic mice, the administration of the long-acting FGF21 analog PF-05231023 reversed diabetes-induced retinal neuronal deficits with improved photoreceptor function and morphology, and decreased photoreceptor-derived inflammation (Fig. 7). PF-05231023 administration suppressed proinflammatory IL-1β expression. IL-1β causes neurovascular damage in the retina (36–38). Therefore, we propose that FGF21 (PF-05231023) regulates retinal NRF2 levels and reduces IL-1β production and photoreceptor dysfunction in DR.

Photoreceptor high-energy consumption makes it susceptible to neurovascular disease. Blood vessels supply nutrients and oxygen to neurons and evacuate waste. Disturbances in neuronal activity trigger vascular remodeling (55). In diabetic animal models, photoreceptor responses to hyperglycemia induce retinal blood vessel loss (6,7,34). In addition, low rod sensitivity is associated with abnormal retinal vasculature.

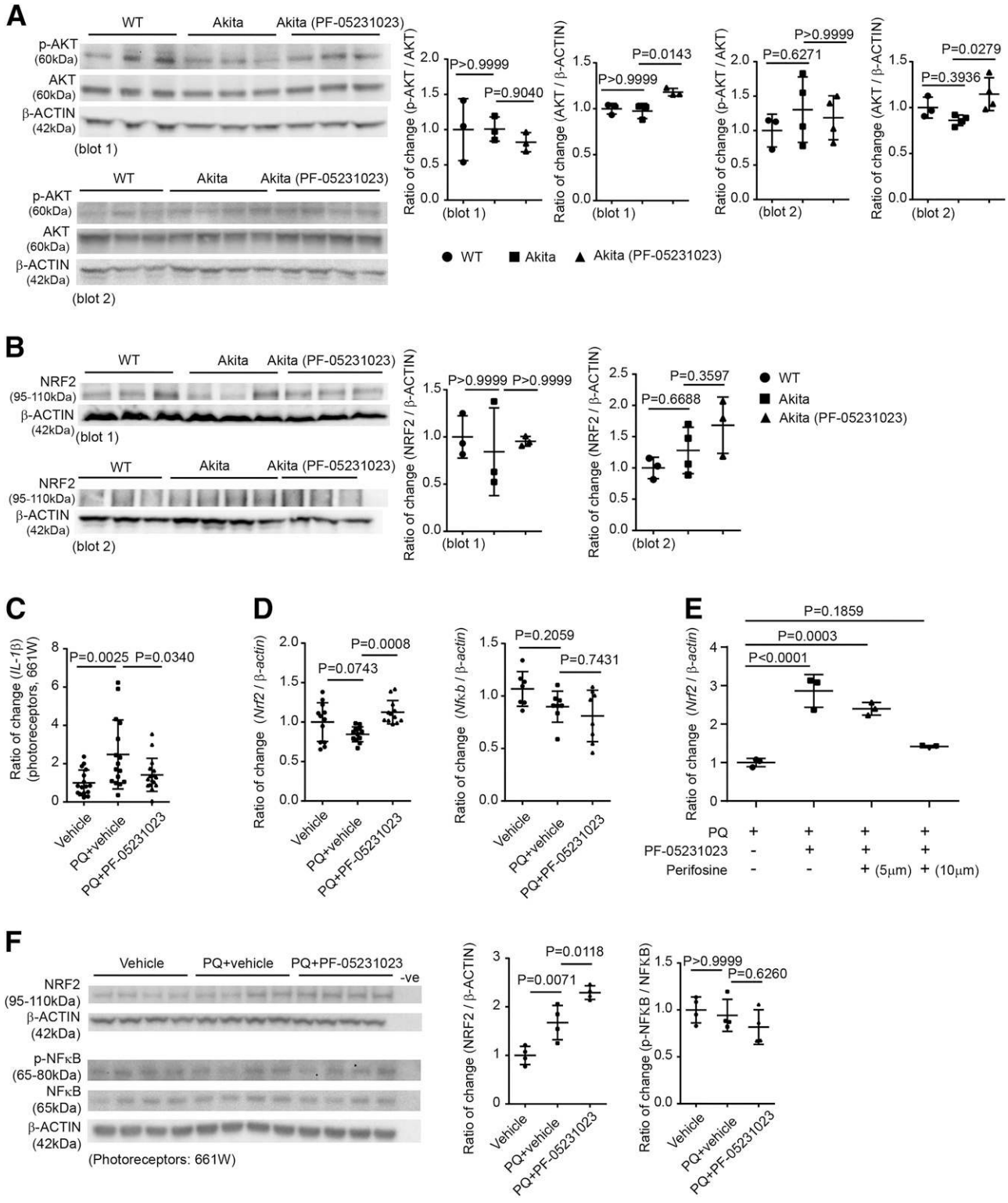

Figure 5—PF-05231023 administration induced NRF2 levels by activating the AKT pathway and decreased photoreceptor-derived IL-1β. *A* and *B*: Western blot of p-AKT, AKT, NRF2 in nondiabetic WT and diabetic Akita mice with vehicle or PF-05231023 administration for 1 month. β-Actin was used as an internal control. The protein level was first compared with internal control. Ratio indicates the ratio of change to β-actin normalized to the WT ratio. Western blot was repeated twice with independent samples. n = 3–4 mice/group per round. ANOVA was used. *C*: qPCR of *IL-1β* in cone photoreceptors in vitro (661 W cells). Oxidative stress was induced with 0.5 mmol/L PQ for 1 h. The culture medium was changed, and cells were treated with 500 ng/mL PF-05231023 or vehicle for 24 h. n = 4 independent replicates. The expression of genes was first compared with internal control *β-actin*. Ratio indicates the ratio of gene to *β-actin* normalized to the control ratio (the non–PQ-treated group). ANOVA followed by Bonferroni multiple comparisons test was used. *D*: qPCR of *Nrf2* and *Nfκb* in 661 W cells with PQ-induced oxidative stress followed by treatment with 500 ng/mL PF-05231023 or vehicle for 24 h. n = 4 independent replicates. The expression of genes was first compared with internal control *β-actin*. Ratio indicates the ratio of gene to β-actin normalized to the control ratio (the non–PQ-treated group). ANOVA followed by Bonferroni

Rod photoreceptor demands contribute to the vascular recovery in hypoxia-induced retinal neovascularization (56). Photoreceptor metabolic dysfunction dictates pathological retinal angiogenesis (57). Therefore, maintaining photoreceptor function may prevent vascular abnormalities in DR. In insulin-deficient Akita mice, we found reduced sensitivity in the postreceptor retina, which is in line with clinical observations (3). Meanwhile, the changes in postreceptor cells were actually reflecting the deficits in photoreceptor function (30,31). We found that the administration of an FGF21 analog, PF-05231023, reversed the diabetes-induced morphological changes in photoreceptors and restored *Sm*; it also reduced disorganization of the photoreceptor segments. This suggests that the effect of PF-05231023 on retinal function ERG may be due to improved photoreceptor structure and function.

There is a strong correlation between hyperglycemia and the development of DR. Hyperglycemia leads to many cellular metabolic alterations that could serve as therapeutic targets. However, although pharmacological interventions disrupt putative biochemical signaling pathways between hyperglycemia and DR, an effective and safe drug is not yet available. Patients with type 1 diabetes have low circulating FGF21 levels (11,12), and FGF21 administration reduces hyperglycemia and lessens renal dysfunction in type 1 diabetic mice (13). FGF21 also improves the lipid profile (i.e., decreased triglycerides) of obese monkeys and patients with type 2 diabetes (58), indicating that FGF21 may have positive effects on diabetes and diabetic complications.

We found no significant impact of PF-05231023 administration on serum triglyceride levels in either Akita or STZ-induced diabetic mice. Although PF-05231023 slightly reduced hyperglycemia in Akita mice, this finding was not replicated in STZ-induced mice. The protective effects of PF-05231023 on retinal neurons is, therefore, likely to be independent of circulating glucose and lipid modulation. We also found that PF-05231023 protection against retinal neuronal deficits was preserved with APN deficiency. In the OIR mouse model of late vasoproliferative retinopathy, FGF21 inhibits pathological neovessel growth mediated by APN (17). Our current findings indicate that FGF21 regulates retinal neuron and neovessel growth through other mechanisms.

Oxidative stress resulting from highly metabolic photoreceptors induces inflammation, which induces DR (6,7,34,35,40). Modulating oxidative stress prevents the progression of DR (43). PF-05231023 administration attenuated the diabetes-induced *IL-1β* expression in Akita mice. FGF21 reduces oxidative stress and inhibits the NF-κB pathway in mice (44). In photoreceptors in vitro with PQ-induced oxidative stress, we observed that PF-05231023 treatment decreased *IL-1β* expression and activated the NRF2 pathway, which is known for its antioxidant capability (41) and for the regulation of *IL-1β* transcription (44,45). Additionally, PF-05231023–induced effect on *IL-1β* was independent of APN in diabetic retinas, which is in line with the neuronal observation. APN inhibits retinal neovessel growth via tumor necrosis factor-α (TNF-α) (59), and FGF21 also reduces TNF-α in neovascular mouse retinas (17). However, in Akita mice, there was no significant change in retinal *Tnfα* expression between PF-05231023– and vehicle-treated groups. Taken together, we concluded that, in diabetic retinas, PF-05231023 protected neuronal activity through the regulation of retinal levels of NRF2 and IL-1β, which was at least to some degree independent of the APN-TNF-α pathway that we showed to be involved in retinal neovascularization in OIR (60). IL-1β causes a decline in mitochondrial membrane potential and ATP production in retinal neurons (36). A reduction of retinal IL-1β may prevent the induction of early vessel loss in DR because *IL-1β* induces retinal microvascular abnormalities in rats (37,38).

In the current study, PF-05231023 was administrated intraperitoneally, and circulating FGF21 levels were measured. PF-05231023 administration did not alter retinal *Fgf21*, *Fgfr1*, and *Klb* expression in Akita mice (Supplementary Fig. 6). These data implicate circulating/peripheral FGF21 as a primary driver of retinal protection rather than autocrine/paracrine effects of FGF21 in the retina. Although FGF21 is expressed in liver, white adipose tissue, and brown adipose tissue, it is a hepatokine, and liver is the primary source of circulating FGF21 under fasting and refeeding conditions (61). In humans, liver is also the primary source of circulating FGF21 in a pattern that is consistent with a hormonal response (62). Although liver-derived FGF21 is critical for the adaptive response to fasting or starvation in rodents, in humans FGF21 plays an important role in fructose metabolism (63). Circulating FGF21 has been shown to cross the blood-brain barrier in humans in a nonsaturable, unidirectional manner (64). FGF21 regulates metabolism and circadian behavior, and sweet and alcohol preferences by directly acting on the nervous system (65,66). The blood-retinal barrier, which is essential for normal visual function (67), is broken down in DR (68). The leaky blood-retinal barrier potentiates the transport of FGF21 from blood into retina. Because local expression of FGF21 receptors has been detected in total retina and in retinal neurons, we speculate that circulating FGF21 could directly act on retinal neurons

multiple-comparisons test was used. *E*: qPCR of *Nrf2* in in 661 W cells with PQ-induced oxidative stress followed by cotreatment with 500 ng/mL PF-05231023 and perifosine at 5 or 10 μmol/L. The expression of genes was first compared with internal control *β-actin*. Ratio indicates the ratio of gene to *β-actin* normalized to control ratio (the non–PQ-treated group). ANOVA was used. *F*: Western blot of NRF2, p–NF-κB, and NF-κB in 661 W cells with PQ-induced oxidative stress followed by treatment with 500 ng/mL PF-05231023 or vehicle for 24 h. Protein lysate was isolated from 661 W cells. β-Actin was used as the internal control. Lane only with loading dye was the negative control. $n = 4$ independent replicates. The protein level was first compared with the internal control. Ratio indicates the ratio of change to β-actin normalized to the control ratio (the non–PQ-treated group). ANOVA followed by Bonferroni multiple-comparisons test was used. Data are presented as the mean ± SD (*A–F*).

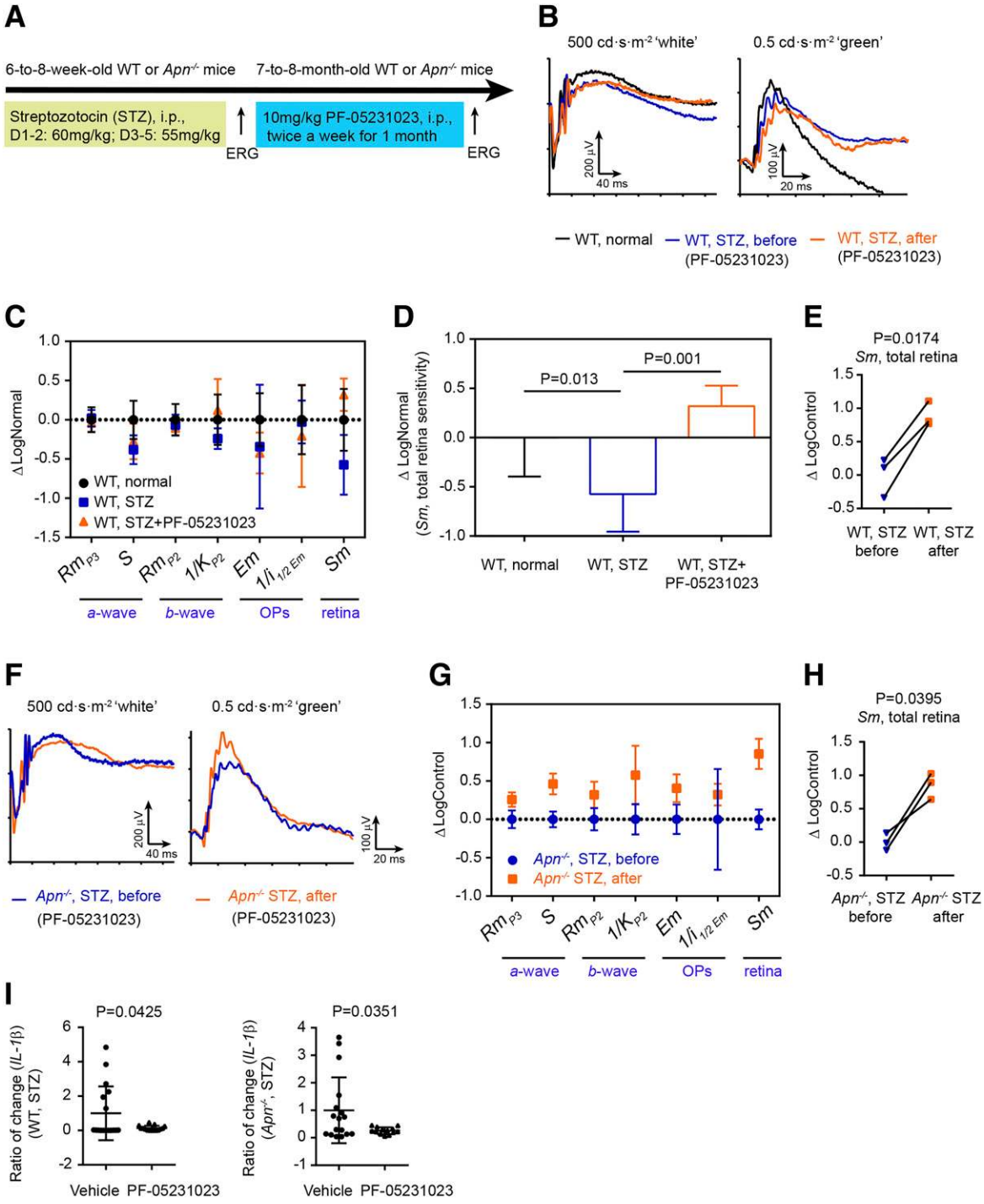

Figure 6—PF-05231023 administration protected the retinal function in STZ-induced diabetic mice, independent of APN. *A*: Schematic of STZ-induced type 1 diabetes in C57BL/6J (WT) mice. STZ was intraperitoneally injected in 6- to 8-week-old WT mice (day 1–2 60 mg/kg; day 3–5 55 mg/kg). ERG was compared in diabetic mice before and after PF-05231023 treatment (10 mg/kg intraperitoneally, twice a week). *B*: Representative ERG plots of 7- to 8-month-old WT control mice and WT diabetic mice before and after PF-05231023 administration. *C*: Overall changes in different ERG parameters in WT normal mice and WT diabetic mice before and after PF-05231023 administration. Rm_{P2}, bipolar cell response amplitude. *D*: Comparison of *Sm* in WT normal mice and WT diabetic mice before and after PF-05231023 administration. n = 6–7 eyes from three to five mice per group. ANOVA followed by Tukey test was used. *E*: Plots of *Sm* in 7- to 8-month-old WT diabetic mice before and after PF-05231023 administration. n = 3 mice/group. Paired t test. *F*: Representative ERG plots of 7- to 8-month-old $Apn^{-/-}$ diabetic mice before and after PF-05231023 administration. *G*: Overall changes in different ERG parameters in $Apn^{-/-}$ diabetic mice before and after PF-05231023 administration. *H*: Plots of *Sm* in $Apn^{-/-}$ diabetic mice before and after PF-05231023 administration. n = 3 mice/group. Paired t test was used. *I*: qPCR for *IL-1β* in diabetic WT and $Apn^{-/-}$ mouse retinas treated with vehicle (PBS) or PF-05231023. n = 13–17 replicates from three mice per group. The expression of genes was first compared with internal control *cyclophilin A*. Ratio indicates the ratio of gene to *cyclophilin A* normalized to WT ratio. Unpaired t test was used. ERG plots with "white" and "green" light stimulation are shown. Data are presented as the mean ± SD.

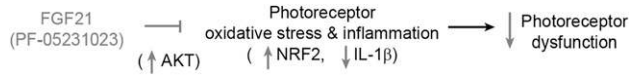

Figure 7—Flowchart for PF-05231023 protection against DR in mice with type 1 diabetes. Schematic of signaling pathway indicating that PF-05231023 may improve retinal neurovascular activity in diabetic mice by inducing antioxidative NRF2 and decreasing photoreceptor-derived proinflammatory marker IL-1β.

to exert protective effects in DR. However, we do not exclude the potential contribution of local FGF21.

Conclusion

In summary, there is an unmet need for the prevention and treatment of DR. Maintaining retinal structure and function, particularly photoreceptor activity, will improve retinal vascular stability, which can be achieved in the following two ways: *1*) modulating photoreceptor metabolism to match the energy supply and *2*) slowing down the visual cycle to reduce the energy demand (69). We determined that FGF21 (independent of VEGFA) may be a novel therapeutic target for the prevention and treatment of DR, possibly through restoring photoreceptor structure and function, and reducing photoreceptor oxidative stress and inflammation. Further exploration of FGF21 effects on photoreceptor metabolism and blood vascular changes in DR is desirable.

Acknowledgments. The authors thank Dr. Jing Chen, Boston Children's Hospital, for her expert advice. The authors also thank Pfizer Cardiovascular and Metabolic Diseases for providing native FGF21 and PF-05231023.

Funding. L.E.H.S. is supported by National Institutes of Health National Eye Institute grants 1R24EY024868 and EY017017, Boston Children's Hospital Intellectual And Developmental Disabilities Research Center grant 1U54-HD-090255, the Lowy Medical Research Institute, and European Commission FP7 project 305485 PREVENT-ROP. A.H. is supported by the Swedish Research Council (DNR# 2011-2432), Gothenburg County Council (grant ALFGBG-426531), long-term support by De Blindas Vänner and Kronprinsessan Margaretas Arbetsnämnd för synskadade, and European Commission FP7 project 305485. Z.F. is supported by the Knights Templar Eye Foundation (grant #76293) and Blind Children's Center (seed grant #89282). C.-H.L. is supported by the Knights Templar Eye Foundation. B.C. is supported by the German Research Foundation (DFG). R.L. is supported by German Research Foundation (DFG) grant Li2650/1-1. Y.S. is supported by a Boston Children's Hospital OFD/BTREC/CTREC Faculty Career Development Grant.

Duality of Interest. S.T. was formerly an employee and stockholder of Pfizer. He is a current employee of Merck and was at the time the study was conducted. No other potential conflicts of interest relevant to this article were reported.

Merck has had no role in any aspects of the work.

Author Contributions. Z.F. contributed to study conception and design; the acquisition, analysis, and interpretation of the data; and the drafting or revision of the article. Z.W., C.-H.L., Y.G., B.C., R.L., Y.S., S.S.M., S.B.B., I.A., E.M., R.D., A.P., and S.S.C. contributed to the acquisition of data. S.T. and A.H. contributed to the drafting or revision of the article. J.D.A. contributed to the analysis and interpretation of the data and the drafting or revision of the article. L.E.H.S. contributed to study conception and design, analysis and interpretation of the data, and the drafting or revision of the article. L.E.H.S. is the guarantor of this work and, as such, had full access to all the data in the study and takes responsibility for the integrity of the data and the accuracy of the data analysis.

Prior Presentation. Parts of this study were presented in abstract form at Cell Symposia: Metabolic Disease Therapies, San Diego, CA, 15–17 October 2017.

References

1. Zheng Y, He M, Congdon N. The worldwide epidemic of diabetic retinopathy. Indian J Ophthalmol 2012;60:428–431
2. Osaadon P, Fagan XJ, Lifshitz T, Levy J. A review of anti-VEGF agents for proliferative diabetic retinopathy. Eye (Lond) 2014;28:510–520
3. Pescosolido N, Barbato A, Stefanucci A, Buomprisco G. Role of electrophysiology in the early diagnosis and follow-up of diabetic retinopathy. J Diabetes Res 2015;2015:319692
4. Kowluru RA, Mishra M. Oxidative stress, mitochondrial damage and diabetic retinopathy. Biochim Biophys Acta 2015;1852:2474–2483
5. Hoang QV, Linsenmeier RA, Chung CK, Curcio CA. Photoreceptor inner segments in monkey and human retina: mitochondrial density, optics, and regional variation. Vis Neurosci 2002;19:395–407
6. Du Y, Veenstra A, Palczewski K, Kern TS. Photoreceptor cells are major contributors to diabetes-induced oxidative stress and local inflammation in the retina. Proc Natl Acad Sci U S A 2013;110:16586–16591
7. Liu H, Tang J, Du Y, et al. Photoreceptor cells influence retinal vascular degeneration in mouse models of retinal degeneration and diabetes. Invest Ophthalmol Vis Sci 2016;57:4272–4281
8. Lahdenranta J, Pasqualini R, Schlingemann RO, et al. An anti-angiogenic state in mice and humans with retinal photoreceptor cell degeneration. Proc Natl Acad Sci U S A 2001;98:10368–10373
9. Dutchak PA, Katafuchi T, Bookout AL, et al. Fibroblast growth factor-21 regulates PPARγ activity and the antidiabetic actions of thiazolidinediones. Cell 2012;148:556–567
10. Owen BM, Mangelsdorf DJ, Kliewer SA. Tissue-specific actions of the metabolic hormones FGF15/19 and FGF21. Trends Endocrinol Metab 2015;26:22–29
11. Zibar K, Blaslov K, Bulum T, Ćuća JK, Smirčić-Duvnjak L. Basal and postprandial change in serum fibroblast growth factor-21 concentration in type 1 diabetic mellitus and in healthy controls. Endocrine 2015;48:848–855
12. Xiao Y, Xu A, Law LS, et al. Distinct changes in serum fibroblast growth factor 21 levels in different subtypes of diabetes. J Clin Endocrinol Metab 2012;97:E54–E58
13. Jiang X, Zhang C, Xin Y, et al. Protective effect of FGF21 on type 1 diabetes-induced testicular apoptotic cell death probably via both mitochondrial- and endoplasmic reticulum stress-dependent pathways in the mouse model. Toxicol Lett 2013;219:65–76
14. Zhang C, Shao M, Yang H, et al. Attenuation of hyperlipidemia- and diabetes-induced early-stage apoptosis and late-stage renal dysfunction via administration of fibroblast growth factor-21 is associated with suppression of renal inflammation. PLoS One 2013;8:e82275
15. Cheng Y, Zhang J, Guo W, et al. Up-regulation of Nrf2 is involved in FGF21-mediated fenofibrate protection against type 1 diabetic nephropathy. Free Radic Biol Med 2016;93:94–109
16. Nakagami Y. Nrf2 is an attractive therapeutic target for retinal diseases. Oxid Med Cell Longev 2016;2016:7469326
17. Fu Z, Gong Y, Liegl R, et al. FGF21 administration suppresses retinal and choroidal neovascularization in mice. Cell Reports 2017;18:1606–1613
18. Lai AK, Lo AC. Animal models of diabetic retinopathy: summary and comparison. J Diabetes Res 2013;2013:106594
19. Lamb TD, Pugh EN Jr. A quantitative account of the activation steps involved in phototransduction in amphibian photoreceptors. J Physiol 1992;449:719–758
20. Wurziger K, Lichtenberger T, Hanitzsch R. On-bipolar cells and depolarising third-order neurons as the origin of the ERG-b-wave in the RCS rat. Vision Res 2001;41:1091–1101
21. Robson JG, Frishman LJ. Response linearity and kinetics of the cat retina: the bipolar cell component of the dark-adapted electroretinogram. Vis Neurosci 1995;12:837–850
22. Fulton AB, Rushton WA. The human rod ERG: correlation with psychophysical responses in light and dark adaptation. Vision Res 1978;18:793–800

23. Dong CJ, Agey P, Hare WA. Origins of the electroretinogram oscillatory potentials in the rabbit retina. Vis Neurosci 2004;21:533–543
24. Lei B, Yao G, Zhang K, Hofeldt KJ, Chang B. Study of rod- and cone-driven oscillatory potentials in mice. Invest Ophthalmol Vis Sci 2006;47:2732–2738
25. Akula JD, Mocko JA, Moskowitz A, Hansen RM, Fulton AB. The oscillatory potentials of the dark-adapted electroretinogram in retinopathy of prematurity. Invest Ophthalmol Vis Sci 2007;48:5788–5797
26. Akula JD, Mocko JA, Benador IY, et al. The neurovascular relation in oxygen-induced retinopathy. Mol Vis 2008;14:2499–2508
27. Fitzmaurice GM, Laird NM, Ware JH. *Applied Longitudinal Analysis*. Hoboken, NJ, Wiley, 2011
28. Foltz IN, Hu S, King C, et al. Treating diabetes and obesity with an FGF21-mimetic antibody activating the βKlotho/FGFR1c receptor complex. Sci Transl Med 2012;4:162ra153
29. Ding X, Boney-Montoya J, Owen BM, et al. βKlotho is required for fibroblast growth factor 21 effects on growth and metabolism. Cell Metab 2012;16:387–393
30. Hansen RM, Moskowitz A, Akula JD, Fulton AB. The neural retina in retinopathy of prematurity. Prog Retin Eye Res 2017;56:32–57
31. Hood DC, Birch DG. A computational model of the amplitude and implicit time of the b-wave of the human ERG. Vis Neurosci 1992;8:107–126
32. Craft CM, Whitmore DH, Wiechmann AF. Cone arrestin identified by targeting expression of a functional family. J Biol Chem 1994;269:4613–4619
33. Deming JD, Pak JS, Brown BM, et al. Visual cone arrestin 4 contributes to visual function and cone health. Invest Ophthalmol Vis Sci 2015;56:5407–5416
34. Tonade D, Liu H, Kern TS. Photoreceptor cells produce inflammatory mediators that contribute to endothelial cell death in diabetes. Invest Ophthalmol Vis Sci 2016;57:4264–4271
35. Joussen AM, Poulaki V, Le ML, et al. A central role for inflammation in the pathogenesis of diabetic retinopathy. FASEB J 2004;18:1450–1452
36. Abcouwer SF, Shanmugam S, Gomez PF, et al. Effect of IL-1beta on survival and energy metabolism of R28 and RGC-5 retinal neurons. Invest Ophthalmol Vis Sci 2008;49:5581–5592
37. Kowluru RA, Odenbach S. Role of interleukin-1beta in the development of retinopathy in rats: effect of antioxidants. Invest Ophthalmol Vis Sci 2004;45:4161–4166
38. Liu Y, Biarnés Costa M, Gerhardinger C. IL-1β is upregulated in the diabetic retina and retinal vessels: cell-specific effect of high glucose and IL-1β autostimulation. PLoS One 2012;7:e36949
39. Madsen-Bouterse SA, Kowluru RA. Oxidative stress and diabetic retinopathy: pathophysiological mechanisms and treatment perspectives. Rev Endocr Metab Disord 2008;9:315–327
40. Kern TS, Berkowitz BA. Photoreceptors in diabetic retinopathy. J Diabetes Investig 2015;6:371–380
41. Xiong W, MacColl Garfinkel AE, Li Y, Benowitz LI, Cepko CL. NRF2 promotes neuronal survival in neurodegeneration and acute nerve damage. J Clin Invest 2015;125:1433–1445
42. Wang L, Chen Y, Sternberg P, Cai J. Essential roles of the PI3 kinase/Akt pathway in regulating Nrf2-dependent antioxidant functions in the RPE. Invest Ophthalmol Vis Sci 2008;49:1671–1678
43. Williams M, Hogg RE, Chakravarthy U. Antioxidants and diabetic retinopathy. Curr Diab Rep 2013;13:481–487
44. Yu Y, He J, Li S, et al. Fibroblast growth factor 21 (FGF21) inhibits macrophage-mediated inflammation by activating Nrf2 and suppressing the NF-κB signaling pathway. Int Immunopharmacol 2016;38:144–152
45. Kobayashi EH, Suzuki T, Funayama R, et al. Nrf2 suppresses macrophage inflammatory response by blocking proinflammatory cytokine transcription. Nat Commun 2016;7:11624
46. McCarthy S, Somayajulu M, Sikorska M, Borowy-Borowski H, Pandey S. Paraquat induces oxidative stress and neuronal cell death; neuroprotection by water-soluble Coenzyme Q10. Toxicol Appl Pharmacol 2004;201:21–31
47. Cogswell JP, Godlevski MM, Wisely GB, et al. NF-kappa B regulates IL-1 beta transcription through a consensus NF-kappa B binding site and a nonconsensus CRE-like site. J Immunol 1994;153:712–723
48. Zitzmann K, Vlotides G, Brand S, et al. Perifosine-mediated Akt inhibition in neuroendocrine tumor cells: role of specific Akt isoforms. Endocr Relat Cancer 2012;19:423–434
49. Birben E, Sahiner UM, Sackesen C, Erzurum S, Kalayci O. Oxidative stress and antioxidant defense. World Allergy Organ J 2012;5:9–19
50. Lin Z, Tian H, Lam KS, et al. Adiponectin mediates the metabolic effects of FGF21 on glucose homeostasis and insulin sensitivity in mice. Cell Metab 2013;17:779–789
51. Holland WL, Adams AC, Brozinick JT, et al. An FGF21-adiponectin-ceramide axis controls energy expenditure and insulin action in mice. Cell Metab 2013;17:790–797
52. Fu Z, Gong Y, Löfqvist C, Hellström A, Smith LE. Review: adiponectin in retinopathy. Biochim Biophys Acta 2016;1862:1392–1400
53. Wong-Riley MT. Energy metabolism of the visual system. Eye Brain 2010;2:99–116
54. Okawa H, Sampath AP, Laughlin SB, Fain GL. ATP consumption by mammalian rod photoreceptors in darkness and in light. Curr Biol 2008;18:1917–1921
55. Fulton AB, Akula JD, Mocko JA, et al. Retinal degenerative and hypoxic ischemic disease. Doc Ophthalmol 2009;118:55–61
56. Akula JD, Hansen RM, Martinez-Perez ME, Fulton AB. Rod photoreceptor function predicts blood vessel abnormality in retinopathy of prematurity. Invest Ophthalmol Vis Sci 2007;48:4351–4359
57. Joyal JS, Sun Y, Gantner ML, et al. Retinal lipid and glucose metabolism dictates angiogenesis through the lipid sensor Ffar1. Nat Med 2016;22:439–445
58. Talukdar S, Zhou Y, Li D, et al. A long-acting FGF21 molecule, PF-05231023, decreases body weight and improves lipid profile in non-human primates and type 2 diabetic subjects. Cell Metab 2016;23:427–440
59. Higuchi A, Ohashi K, Kihara S, Walsh K, Ouchi N. Adiponectin suppresses pathological microvessel formation in retina through modulation of tumor necrosis factor-alpha expression. Circ Res 2009;104:1058–1065
60. Fu Z, Lofqvist CA, Shao Z, et al. Dietary ω-3 polyunsaturated fatty acids decrease retinal neovascularization by adipose-endoplasmic reticulum stress reduction to increase adiponectin. Am J Clin Nutr 2015;101:879–888
61. Markan KR, Naber MC, Ameka MK, et al. Circulating FGF21 is liver derived and enhances glucose uptake during refeeding and overfeeding. Diabetes 2014;63:4057–4063
62. Yang C, Lu W, Lin T, et al. Activation of Liver FGF21 in hepatocarcinogenesis and during hepatic stress. BMC Gastroenterol 2013;13:67
63. Dushay JR, Toschi E, Mitten EK, Fisher FM, Herman MA, Maratos-Flier E. Fructose ingestion acutely stimulates circulating FGF21 levels in humans. Mol Metab 2014;4:51–57
64. Hsuchou H, Pan W, Kastin AJ. The fasting polypeptide FGF21 can enter brain from blood. Peptides 2007;28:2382–2386
65. Bookout AL, de Groot MH, Owen BM, et al. FGF21 regulates metabolism and circadian behavior by acting on the nervous system. Nat Med 2013;19:1147–1152
66. Talukdar S, Owen BM, Song P, et al. FGF21 regulates sweet and alcohol preference. Cell Metab 2016;23:344–349
67. Cunha-Vaz J. The blood-retinal barrier in the management of retinal disease: EURETINA award lecture. Ophthalmologica 2017;237:1–10
68. Klaassen I, Van Noorden CJ, Schlingemann RO. Molecular basis of the inner blood-retinal barrier and its breakdown in diabetic macular edema and other pathological conditions. Prog Retin Eye Res 2013;34:19–48
69. Liu H, Tang J, Du Y, et al. Retinylamine benefits early diabetic retinopathy in mice. J Biol Chem 2015;290:21568–21579